Research Article | Vol. 9, No. 4 | 1 Apr 2018 | BIOMEDICAL OPTICS EXPRESS 1692
Biomedical Optics EXPRESS

Label-free light-sheet microfluidic cytometry for the automatic identification of senescent cells

MEIAI LIN,[1] QIAO LIU,[2,3] CHAO LIU,[1] XU QIAO,[1] CHANGSHUN SHAO,[2,3] AND XUANTAO SU[1,*]

[1]*Institute of Biomedical Engineering, School of Control Science and Engineering, Shandong University, Jinan, Shandong, 250061, China*
[2]*Department of Molecular Medicine and Genetics, School of Basic Medicine, Shandong University, Jinan, Shandong, 250012, China*
[3]*Key Laboratory of Experimental Teratology (Ministry of Education), Shandong University, Jinan, Shandong, 250012, China*
**xtsu@sdu.edu.cn*

Abstract: Label-free microfluidic cytometry is of increasing interest for single cell analysis due to its advantages of high-throughput, miniaturization, as well as noninvasive detection. Here we develop a next generation label-free light-sheet microfluidic cytometer for single cell analysis by two-dimensional (2D) light scattering measurements. Our cytometer integrates light sheet illumination with a disposable hydrodynamic focusing unit, which can achieve 3D hydrodynamic focusing of a sample fluid to a diameter of 19 micrometer without microfabrication. This integration also improves the signal to noise ratio (SNR) for the acquisition of 2D light scattering patterns from label-free cells. Particle sizing with submicron resolution is achieved by our light-sheet flow cytometer, where Euclidean distance-based similarity measures are performed. Label-free, automatic classification of senescent and normal cells is achieved with a high accuracy rate by incorporating our light-sheet flow cytometry with support vector machine (SVM) algorithms. Our light-sheet microfluidic cytometry with a microfabrication-free hydrodynamic focusing unit may find wide applications for automatic and label-free clinical diagnosis.

OCIS codes: (170.3890) Medical optics instrumentation; (170.4580) Optical diagnostics for medicine; (170.1530) Cell analysis; (120.5820) Scattering measurements.

References and links

1. M. Collado, M. A. Blasco, and M. Serrano, "Cellular senescence in cancer and aging," Cell **130**(2), 223–233 (2007).
2. B. G. Childs, M. Durik, D. J. Baker, and J. M. van Deursen, "Cellular senescence in aging and age-related disease: from mechanisms to therapy," Nat. Med. **21**(12), 1424–1435 (2015).
3. E. S. Hwang, G. Yoon, and H. T. Kang, "A comparative analysis of the cell biology of senescence and aging," Cell. Mol. Life Sci. **66**(15), 2503–2524 (2009).
4. G. P. Dimri, X. Lee, G. Basile, M. Acosta, G. Scott, C. Roskelley, E. E. Medrano, M. Linskens, I. Rubelj, and O. Pereira-Smith, "A biomarker that identifies senescent human cells in culture and in aging skin in vivo," Proc. Natl. Acad. Sci. U.S.A. **92**(20), 9363–9367 (1995).
5. E. Sikora, T. Arendt, M. Bennett, and M. Narita, "Impact of cellular senescence signature on ageing research," Ageing Res. Rev. **10**(1), 146–152 (2011).
6. F. Debacq-Chainiaux, J. D. Erusalimsky, J. Campisi, and O. Toussaint, "Protocols to detect senescence-associated beta-galactosidase (SA-betagal) activity, a biomarker of senescent cells in culture and in vivo," Nat. Protoc. **4**(12), 1798–1806 (2009).
7. M. Monici, "Cell and tissue autofluorescence research and diagnostic applications," in *Biotechnology Annual Review* (Elsevier, 2005), pp. 227–256.
8. S. He, C. Ye, Q. Sun, C. K. S. Leung, and J. Y. A. Qu, "Label-free nonlinear optical imaging of mouse retina," Biomed. Opt. Express **6**(3), 1055–1066 (2015).
9. L. Wei, F. Hu, Y. Shen, Z. Chen, Y. Yu, C.-C. Lin, M. C. Wang, and W. Min, "Live-cell imaging of alkyne-tagged small biomolecules by stimulated Raman scattering," Nat. Methods **11**(4), 410–412 (2014).

#318261 https://doi.org/10.1364/BOE.9.001692
Journal © 2018 Received 21 Dec 2017; revised 3 Mar 2018; accepted 3 Mar 2018; published 14 Mar 2018

Biomedical Optics EXPRESS

10. C. Zhang, K.-C. Huang, B. Rajwa, J. Li, S. Yang, H. Lin, C. Liao, G. Eakins, S. Kuang, V. Patsekin, J. P. Robinson, and J.-X. Cheng, "Stimulated Raman scattering flow cytometry for label-free single-particle analysis," Optica **4**(1), 103–109 (2017).
11. V. Backman, M. B. Wallace, L. T. Perelman, J. T. Arendt, R. Gurjar, M. G. Müller, Q. Zhang, G. Zonios, E. Kline, J. A. McGilligan, S. Shapshay, T. Valdez, K. Badizadegan, J. M. Crawford, M. Fitzmaurice, S. Kabani, H. S. Levin, M. Seiler, R. R. Dasari, I. Itzkan, J. Van Dam, and M. S. Feld, "Detection of preinvasive cancer cells," Nature **406**(6791), 35–36 (2000).
12. T. E. Matthews, M. Medina, J. R. Maher, H. Levinson, W. J. Brown, and A. Wax, "Deep tissue imaging using spectroscopic analysis of multiply scattered light," Optica **1**(2), 105–111 (2014).
13. E. Luther, L. P. Mendes, J. Pan, D. F. Costa, and V. P. Torchilin, "Applications of Label-Free, Quantitative Phase Holographic Imaging Cytometry to the Development of Multi-Specific Nanoscale Pharmaceutical Formulations," Cytometry A **91**(5), 412–423 (2017).
14. F. Merola, P. Memmolo, L. Miccio, R. Savoia, M. Mugnano, A. Fontana, G. D'Ippolito, A. Sardo, A. Iolascon, A. Gambale, and P. Ferraro, "Tomographic flow cytometry by digital holography," Light Sci. Appl. **6**(4), 16241–16247 (2017).
15. D. Psaltis, S. R. Quake, and C. Yang, "Developing optofluidic technology through the fusion of microfluidics and optics," Nature **442**(7101), 381–386 (2006).
16. A. Q. Liu, H. J. Huang, L. K. Chin, Y. F. Yu, and X. C. Li, "Label-free detection with micro optical fluidic systems (MOFS): a review," Anal. Bioanal. Chem. **391**(7), 2443–2452 (2008).
17. J. Emmelkamp, F. Wolbers, H. Andersson, R. S. Dacosta, B. C. Wilson, I. Vermes, and A. van den Berg, "The potential of autofluorescence for the detection of single living cells for label-free cell sorting in microfluidic systems," Electrophoresis **25**(21-22), 3740–3745 (2004).
18. G. L. Liu and L. P. Lee, "Nanowell surface enhanced Raman scattering arrays fabricated by soft-lithography for label-free biomolecular detections in integrated microfluidics," Appl. Phys. Lett. **87**, 074101 (2005).
19. D. Dannhauser, D. Rossi, P. Memmolo, F. Causa, A. Finizio, P. Ferraro, and P. A. Netti, "Label-free analysis of mononuclear human blood cells in microfluidic flow by coherent imaging tools," J. Biophotonics **10**(5), 683–689 (2017).
20. X.-T. Su, K. Singh, C. Capjack, J. Petrácek, C. Backhouse, and W. Rozmus, "Measurements of light scattering in an integrated microfluidic waveguide cytometer," J. Biomed. Opt. **13**(2), 024024 (2008).
21. X.-T. Su, C. Capjack, W. Rozmus, and C. Backhouse, "2D light scattering patterns of mitochondria in single cells," Opt. Express **15**(17), 10562–10575 (2007).
22. S. K. Yarmoska, S. Kim, T. E. Matthews, and A. Wax, "A scattering phantom for observing long range order with two-dimensional angle-resolved Low-Coherence Interferometry," Biomed. Opt. Express **4**(9), 1742–1748 (2013).
23. D. Arifler, C. Macaulay, M. Follen, and M. Guillaud, "Numerical investigation of two-dimensional light scattering patterns of cervical cell nuclei to map dysplastic changes at different epithelial depths," Biomed. Opt. Express **5**(2), 485–498 (2014).
24. G. M. Whitesides, "The origins and the future of microfluidics," Nature **442**(7101), 368–373 (2006).
25. J. Godin, C.-H. Chen, S. H. Cho, W. Qiao, F. Tsai, and Y.-H. Lo, "Microfluidics and photonics for Bio-System-on-a-Chip: A review of advancements in technology towards a microfluidic flow cytometry chip," J. Biophotonics **1**(5), 355–376 (2008).
26. M. E. Piyasena and S. W. Graves, "The intersection of flow cytometry with microfluidics and microfabrication," Lab Chip **14**(6), 1044–1059 (2014).
27. J. Huisken, J. Swoger, F. Del Bene, J. Wittbrodt, and E. H. K. Stelzer, "Optical sectioning deep inside live embryos by selective plane illumination microscopy," Science **305**(5686), 1007–1009 (2004).
28. R. Regmi, K. Mohan, and P. P. Mondal, "MRT Letter: Light Sheet Based Imaging Flow Cytometry on a Microfluidic Platform," Microsc. Res. Tech. **76**(11), 1101–1107 (2013).
29. H. Deschout, K. Raemdonck, S. Stremersch, P. Maoddi, G. Mernier, P. Renaud, S. Jiguet, A. Hendrix, M. Bracke, R. Van den Broecke, M. Röding, M. Rudemo, J. Demeester, S. C. De Smedt, F. Strubbe, K. Neyts, and K. Braeckmans, "On-chip light sheet illumination enables diagnostic size and concentration measurements of membrane vesicles in biofluids," Nanoscale **6**(3), 1741–1747 (2014).
30. H. Jiang, T. Zhu, H. Zhang, J. Nie, Z. Guan, C.-M. Ho, S. Liu, and P. Fei, "Droplet-based light-sheet fluorescence microscopy for high-throughput sample preparation, 3-D imaging and quantitative analysis on a chip," Lab Chip **17**(13), 2193–2197 (2017).
31. L. Ouldarbi, G. Pérret, P. Lemaitre, E. Porcheron, S. Coëtmellec, G. Gréhan, D. Lebrun, and M. Brunel, "Simultaneous 3D location and size measurement of bubbles and sand particles in a flow using interferometric particle imaging," Appl. Opt. **54**(25), 7773–7780 (2015).
32. X. Su, S. E. Kirkwood, M. Gupta, L. Marquez-Curtis, Y. Qiu, A. Janowska-Wieczorek, W. Rozmus, and Y. Y. Tsui, "Microscope-based label-free microfluidic cytometry," Opt. Express **19**(1), 387–398 (2011).
33. L. Xie, Q. Liu, C. Shao, and X. Su, "Differentiation of normal and leukemic cells by 2D light scattering label-free static cytometry," Opt. Express **24**(19), 21700–21707 (2016).
34. C. J. Engelbrecht and E. H. K. Stelzer, "Resolution enhancement in a light-sheet-based microscope (SPIM)," Opt. Lett. **31**(10), 1477–1479 (2006).

Biomedical Optics EXPRESS

35. Z. Wei, H. Guo, Z. Liu, X. Zhang, Q. Liu, Y. Qian, Y. Gong, and C. Shao, "CUL4B impedes stress-induced cellular senescence by dampening a p53-reactive oxygen species positive feedback loop," Free Radic. Biol. Med. **79**, 1–13 (2015).
36. C. J. Burges, "A tutorial on support vector machines for pattern recognition," Data Min. Knowl. Discov. **2**(2), 121–167 (1998).
37. M. Lin, X. Qiao, Q. Liu, C. Shao, and X. Su, "Light-sheet-based 2D light scattering cytometry for label-free characterization of senescent cells," Biomed. Opt. Express **7**(12), 5170–5181 (2016).
38. L. K. Soh and C. Tsatsoulis, "Texture analysis of SAR sea ice imagery using gray level co-occurrence matrices," IEEE. T. Geosci. Remote **37**(2), 780–795 (1999).
39. H. M. Shapiro, *Practical Flow cytometry* (John Wiley & Sons, 2005).
40. B. K. Mckenna, A. A. Selim, F. Richard Bringhurst, and D. J. Ehrlich, "384-Channel parallel microfluidic cytometer for rare-cell screening," Lab Chip **9**(2), 305–310 (2009).

1. Introduction

Identification of senescent cells is important for the better understanding of aging, cancer and many other age-related diseases [1, 2]. When cells undergo senescence, a series of morphological changes and functional alterations occur, such as proliferation termination and apoptosis resistance [3]. Conventionally, cell senescence are characterized by histochemical or fluorescence-based detection of biomarkers [4, 5]. For example, the activity of SA-β-gal (a widely used biomarker for senescent cells) can be measured by using flow cytometry with fluorescence reagents [6]. However commercially available flow cytometer is bulky and expensive, and the routine operation of a cytometer is complex and requires skilled personnel. Furthermore, the fluorescence-based detection relies on specific biomarkers of cells to perform characterization, which is sophisticated and time-consuming. Thus the wide adoption of flow cytometer for cell analysis is limited. There is a great need to develop label-free microfluidic device because of its high-throughput, miniaturization, as well as non-invasive detection for single-cell analysis.

Label-free single cell analysis has been performed by measurements of the optical properties of cells, including autofluorescence [7, 8], Raman scattering [9, 10] and elastic light scattering [11, 12], and digital holography [13, 14]. In order to develop high-throughput, miniaturized devices for the measurements of optical signals from cells, there are recent advancements of integration of optics (micro-optics) with microfluidics [15, 16]. For example, the combination of cellular autofluorescence with microfluidic device showed the potential for detection of living cells [17]. The surface enhanced Raman scattering was integrated into a microfluidic chip to enable the detection of biomolecules [18]. David Dannhauser et al. have integrated the digital holographic technique and light scattering into microfluidic cytometry to characterize flowing cells [19]. Su et al. have recently developed the light scattering microfluidic cytometry for label-free single cell analysis by measurements of the two-dimensional (2D) light scattering patterns [20]. The 2D patterns are sensitive to the cellular microstructures and organelles such as nucleus and mitochondria [21–23].

Compared with autofluorescence and Raman scattering, elastic light scattering provides a more direct observation of the optical signals from cells. However the elastic light scattering measurements require a high signal-to-noise ratio (SNR) because the scattered lights have the same frequency from both the object and the background, especially for single cell analysis in a microfluidic flow. To solve this problem, researchers have explored various approaches to improve the SNR of elastic light scattering measurements. One strategy is to design special microfabricated structures for background noise suppression. For instance, a microsized observation window was fabricated on a coated glass slide that serves as an aperture to improve the SNR for light scattering measurements [21]. Secondly, sheath fluid technology can make cells flow in single profiles along a focused stream that is away from the microchannel side walls. This can effectively suppress the background noise caused by channel-sheath interfaces and other scatterers in the microfluidic channel. With the advancement of microfabrication technology, complex microchannel structures can be

Biomedical Optics EXPRESS

achieved to generate sheath flows [24–26]. However this technology has a high demanding for microfabrication instruments that are not always readily accessible.

Another solution to improve SNR of light scattering detection is to modify the illumination beam. A "beam-in-liquid" structure was built to directly guide the illumination beam into a sample fluid to reduce the background noise due to the refractive index mismatch at sample-medium interface [20]. Light sheet technology has recently been developed to improve the fluorescent detection, where only the fluorescent labels that are within the focused plane can be excited [27]. This technique has lately been incorporated into microfluidic devices for better planar illumination or optical sectioning [28–30]. We expect that the light sheet technology may help to improve the SNR of light scattering microfluidic cytometry.

In this work, we develop the label-free light-sheet microfluidic cytometry for particle sizing and senescent cell identification. Different from conventional microfluidic channels, a compact hydrodynamic focusing unit which is free of microfabrication was developed. This unit enables the hydrodynamic focusing of individual flowing scattterers and enhances the SNR for light scattering measurements. In our microfluidic cytometer, 3D hydrodynamic focusing can be achieved with a sample fluid focused to approximately 19 μm in width. For better excitation of single cells or particles flowing within a narrow microfluidic channel, light sheet technique is integrated with the hydrodynamic focusing unit to provide a uniform illumination. This is particularly suitable for light scattering detection when an optical objective with low numerical aperture (NA) is used for defocused imaging. In our experiments, 2D light scattering patterns from single scatterers are captured by a CMOS sensor via an objective (10x) with an NA of 0.25.

Measurements of microspheres with a standard deviation (SD) of 250 nm were performed by our label-free light-sheet microfluidic cytometry. The agreements between experimental 2D light scattering patterns of microspheres and Mie theory simulations validate the operation as well as the sensitivity of our cytometer with a microfabrication-free hydrodynamic focusing unit. Conventionally, the best resolution that can be achieved for an objective with an NA of 0.25 is about 1340 nm with visible light illumination. Previously, we have developed a Fourier transform method for particle sizing in a microfluidic flow by analyzing the 2D light scattering patterns [20]. Recently, interferometric particle imaging has been developed for particle sizing of transparent bubbles in a flow [31]. Here we developed a novel method that can be used for submicron particle sizing of the microspheres with a SD of 250 nm by Euclidean distance-based similarity measurements. By using our light-sheet microfluidic cytometer, we obtained 2D light scattering patterns of normal human fibroblasts (NHFs) and senescent human fibroblasts (SHFs) in flow. The 2D patterns are analyzed by using the gray-level co-occurrence matrices (GLCM) method for texture description. Support vector machine (SVM) algorithm is used for automatic classification of the normal and senescent cells, and a classification accuracy rate of 88% is obtained. Our results demonstrate that the light-sheet microfluidic cytometry with a microfabrication-free hydrodynamic focusing unit may be used for label-free analysis of senescence-related disease.

2. Materials and method

A schematic diagram of our label-free light-sheet microfluidic cytometer with a microfabrication-free hydrodynamic focusing unit is illustrated in Fig. 1. A laser beam with a wavelength of 532 nm is generated from a diode pumped solid state (DPSS) laser (Frankfurt, Germany) and is filtered by a neutral density (ND) filter (Thorlabs, USA). The incident laser beam is projected on a cylindrical lens (CL) with a focal length of 150 mm (Thorlabs, USA), which is manipulated into a light sheet. A slit is added to adjust the width of the light sheet. This light sheet with a controllable thickness is used to excite the single cells/particles flowing in the hydrodynamic focusing unit that is positioned on a translation stage (TS) (Thorlabs, USA). Two syringe pumps are connected to this unit in order to drive the sample

Biomedical Optics EXPRESS

fluid and sheath fluid. The 2D light scattering patterns from individual single flowing scatterers are imaged by a CMOS sensor (Canon, Japan), which has a maximum resolution of 5184 x 3456 pixels with the pixel size of 4.3 μm, via a 10x objective lens (Olympus, Japan) with an NA of 0.25. In this flowing mode, the resolution of the CMOS sensor that we used is 1920 x 1080 pixels. Finally, the experimental 2D patterns are sent to a data processor for further analysis.

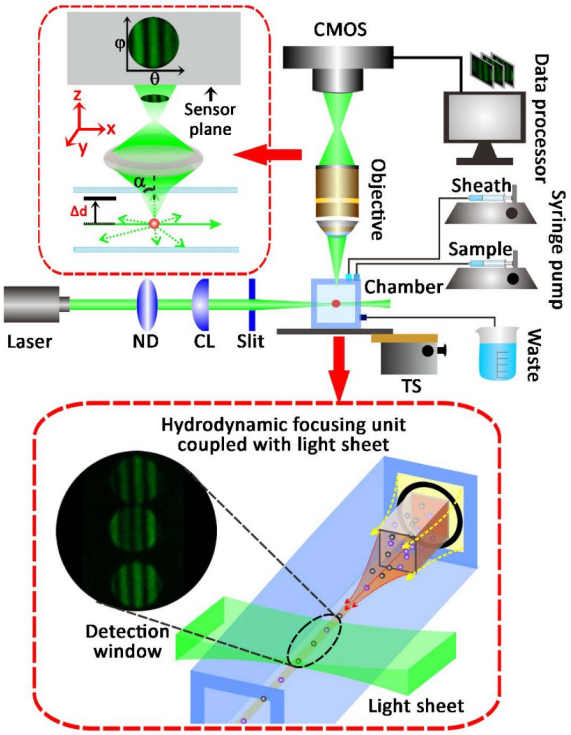

Fig. 1. Illustration of the label-free light-sheet microfluidic cytometer. The collimated laser beam is incident on a cylindrical lens (CL), which reshapes the beam into a light sheet. The single cells/particles flowing in the sample chamber, which is placed on a translation stage (TS), are excited by this light sheet. Two syringe pumps are used to drive the sample fluid and the sheath fluid. The 2D light scattering patterns are captured by a CMOS sensor via an objective and then sent to the data processor for analysis. The acquisition of the 2D light scattering patterns is illustrated in detail (top inset picture). A single scatterer is excited by a laser light, whose scattered light is recorded as a 2D pattern by a CMOS sensor via an objective working in defocusing mode, where the imaging plane is further away from sample plane by Δd. A detailed illustration of the hydrodynamic focusing unit coupled with light sheet is shown in the bottom inset picture. The inner capillary serves as the microchannel for sample fluid and the outer one is used as the sheath fluid channel. The flowing cells passing through the detection window are excited by a uniform light-sheet beam.

The rationale for the acquisition of 2D light scattering patterns from single cells is depicted in Fig. 1 (top inset picture). An incident polarized laser beam propagating along positive X-axis illuminates a single scatterer. The scattered light distribution varies with both polar angle θ and azimuthal angle φ, which is collected by an objective lens onto a 2D CMOS sensor. It should be noticed that the objective here is working in a defocusing mode, and the defocusing distance is Δd [20]. The detection angular range of θ and φ is mainly determined by the numerical aperture (NA) of the objective. More information regarding the optical theory for 2D light scattering patterns can be found in our previous publications [32, 33]. In

Biomedical Optics EXPRESS

this work, the objective with an NA of 0.25 determines the half-angle α to be around 11°, and the corresponding ranges for θ and φ are both from approximately 79° to 101°. For the simulation of 2D light scattering from spherical beads, a code based on Mie theory was developed for the optical layout of our cytometer shown in Fig. 1.

The core part of our label-free microfluidic cytometer is the microfabrication-free hydrodynamic focusing unit coupled with the light sheet illumination, which is presented in Fig. 1 (bottom inset picture). Two glass capillaries are assembled coaxially and fixed by using a specially designed ring that matches well with the size of the capillaries. The inner capillary serves as the channel for sample fluid while the outer one provides channel for sheath fluid. It is critical to make the inner capillary right at the centre of the outer one so that a steady 3D hydrodynamic focusing flow can occur. Glass capillaries with different dimensions can be selected in accordance to specific applications of our disposable hydrodynamic focusing unit. The width of the focused stream depends on the relative pressure between the sample fluid and sheath fluid, which will be demonstrated later in this work.

3. Results

3.1 Measurements of the 3D focused stream generated by the disposable hydrodynamic focusing unit

In order to analyze the hydrodynamic focusing effect of our hydrodynamic focusing unit, the Rhodamine 6G fluorescent dye (Life Technologies, USA) which has an excitation wavelength of 535 nm and an emission wavelength of 575 nm was used for visualization of the focused stream profile. The fluorescent dye was diluted by using ultrapure water, with a concentration of 2.61 μM. Because the width of the focused stream is mainly determined by the relative pressure between sample fluid and sheath fluid, we controlled the flow rates of the syringe pumps to achieve various pressures. In this work, the flow rate Q_{in} of the syringe pump was set to 2 μL/min to drive sample solution, while the flow rate Q_{out} of the pump for driving sheath fluid was changed from 1 to 1000 times (2 to 2000 μL/min) of Q_{in}. As shown in Figs. 2(a)-(c), the different widths of sample stream in the microfluidic channel are obtained for different relative flow rate ratios ΔQ (which is defined as Q_{out} divided by Q_{in}) of 50, 100 and 1000, respectively. It can be seen that when ΔQ increases, the fluid narrows into a focused stream with smaller diameter.

The effect of inject sample fluid diameter on the hydrodynamic focusing was also studied. The profile of the hydrodynamically focused stream when ΔQ reaches 1000 is visualized in Fig. 2(d) for the inner glass capillary with an inner diameter of 50 μm. The widths of the hydrodynamic focused stream with different flow rate ratios for two inner glass capillaries are shown in Fig. 2(e). For the capillary with an inner diameter of 100 μm, the width measured at ΔQ of 50 is about 93 μm, at ΔQ of 100 is 57 μm, and then the width becomes less than 20 μm when ΔQ reaches 1000. The performance for the 50 μm capillary has similar overall tendency, with little discrepancy for ΔQ less than 300. Especially, the widths for both capillaries achieve less than 20 μm when ΔQ reaches 1000. In this work, the disposable hydrodynamic focusing unit was made by using the glass capillary with an inner diameter of 100 μm as sample fluid channel if not otherwise specified.

The sample fluid velocity varying with flow rate ratio ΔQ was measured and is illustrated in Fig. 2(f), where the measured data is marked as triangle symbols and fitted by a polynomial function. It is known that when the width of sample fluid narrows, the velocity of the focused stream increases. As expected, the sample fluid speeds up polynomially when the flow rate ratio increases. As shown in Fig. 2(f), the speed of the focused sample fluid is about 3.15 mm/s when ΔQ is 100. In the following experiments, the flow rate ratio ΔQ of sheath to sample fluid was set to be 100. In this case, the detection of more than 25 cells per second can be achieved.

Biomedical Optics EXPRESS

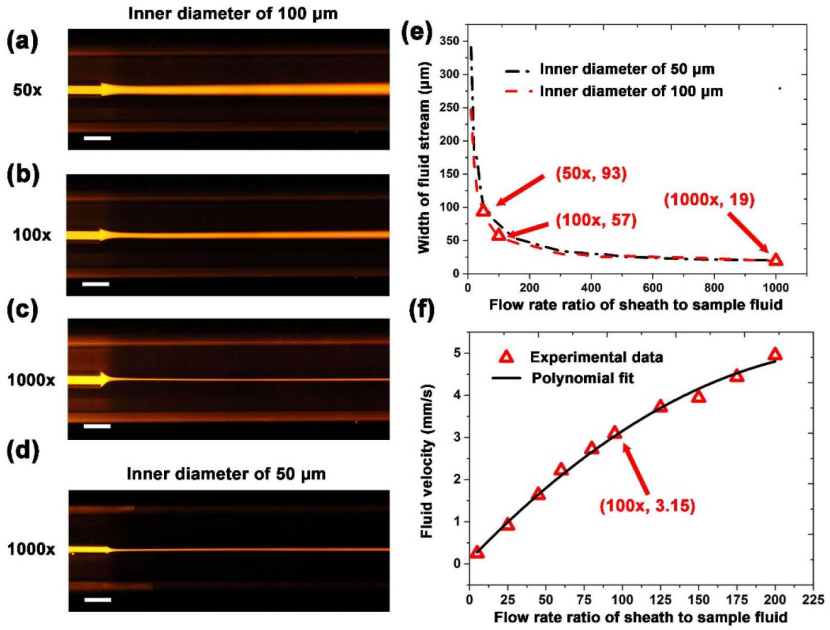

Fig. 2. Measurements of the stream focusing effects of the hydrodynamic focusing unit. Figures (a)-(c) show the observations of the focused stream generated with the sample fluid channel of 100 μm in diameter. The flow rate ratio of the sheath to sample fluid is 50 for (a), 100 for (b) and 1000 for (c), respectively. (d) is the result for the sample fluid channel of 50 μm in diameter when the flow rate ratio is 1000. Scale bar: 300 μm. The focused stream width variation with the flow rate ratio is shown in (e). The measurements of (a) (b) (c) are marked as triangle symbols in (e). Figure (f) shows the measured focused sample fluid velocity varying with flow rate ratio. The experimental data are denoted by triangle symbols and the solid line is a polynomial fit.

3.2 Characterization of light-sheet illumination

The flexible control of beam thickness makes light sheet a decent alternative excitation method particularly for light scattering microfluidic cytometry. Here we adopt light-sheet excitation method to provide uniform illumination of single scatterers flowing within the 3D hydrodynamically focused stream. As the width of the focused sample fluid stream is around 57 μm, the thickness of the light sheet is controlled to be around this value to cover the cross-section of the focused sample fluid. It has been reported that the dimension of light sheet is mainly determined by the focal length of the cylindrical lens, and the width of light beam that is incident on this lens [34]. In our cytometer, the focal length of the lens is 150 mm and the diameter of the laser beam incident on the lens is about 1.1 mm. This gives a light sheet with a thickness of 54 μm theoretically at full width at half maximum (FWHM).

In order to measure the experimental thickness of the light sheet, Rhodamine 6G solution was used for the visualization of the light sheet profile. The result is shown in Fig. 3(a), where the width of the light-sheet beam along the dashed line is measured to be 55 μm (FWHM), as plotted in Fig. 3(b). The confocal parameter that describes the distance while the light sheet propagates almost uniformly is 20 mm. This means that light sheet can provide a uniform illumination that is long enough to adapt to the detection objective. In this work the light sheet has a thickness (Z-direction) of 55 μm, a width (Y-direction) of 1.1 mm, and a uniform propagation length (X-direction) of 20 mm. A slit can be added into the optical path to control the width of the light sheet for specific requirements.

Biomedical Optics EXPRESS

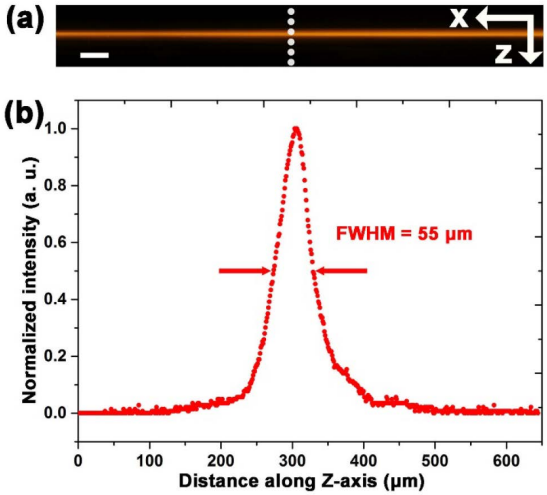

Fig. 3. Measurement of the light sheet thickness that is adapted to the diameter of the focused stream. Figure (a) is the light sheet profile visualized with Rhodamine 6G solution. Scale bar: 300 μm. Figure (b) shows the thickness of the light sheet measured at the FWHM along the dotted line in (a).

3.3 Bead size evaluation by using a light-sheet microfluidic cytometer

In order to demonstrate the sensitivity of our label-free light-sheet microfluidic cytometer, standard polystyrene microspheres (Bangs Laboratories, USA) that have a mean diameter of 3.87 μm and an SD of 250 nm were used in this work. The microspheres were diluted with ultrapure water and sonicated for 5 minutes. The concentration of the microspheres in diluted solution that we used in this work was around 6 x 10^5/mL. The prepared bead solution was driven by a syringe pump with a flow rate of 2 uL/min. Ultrapure water was used as sheath fluid and pumped by another syringe, with a flow rate of 200 μL/min. Before obtaining of the 2D light scattering patterns, the sample stream was aligned to be within the light sheet illumination plane for optimized observation. In our experiments, the 2D light scattering patterns of beads were obtained when the objective was working in defocusing mode with a defocusing distance of about 500 μm. The 2D patterns were recorded continuously at 25 frames/s by using a CMOS detector with an integration time of 1/300 s. The flowing scatterer can be treated as relatively static considering the flow rate of 3.15 mm/s when obtaining its 2D light scattering pattern with such a short integration time. The hydrodynamic focusing confines the scatterers well along the central line of the CMOS sensor, and the 2D light scattering patterns are extracted symmetrically about the 90 degree light scattering. Thus the shift of cell will barely affect the light scattering angular ranges of the 2D patterns. Two-dimensional light scattering patterns (200 x 200 pixels) with about 9 pixels per degree in the polar angular range from 79 to 101 degrees were extracted from the video. And there were 1600 frames extracted from the video of 64 s. From these frames, we obtained 210 light scattering patterns of beads. Fig. 4(a) and Fig. 4(e) show the representative results. It can be seen that the light scattering patterns from the 3.87 μm microspheres present distinct fringe distributions, which indicates the size discrepancy because of the fact that the microspheres differ in diameter with an SD of 250 nm. This demonstrates that our light-sheet microfluidic cytometer has capability to obtain 2D patterns from flowing scatterers with decent quality and may serve for particle sizing with submicron resolution.

Biomedical Optics EXPRESS

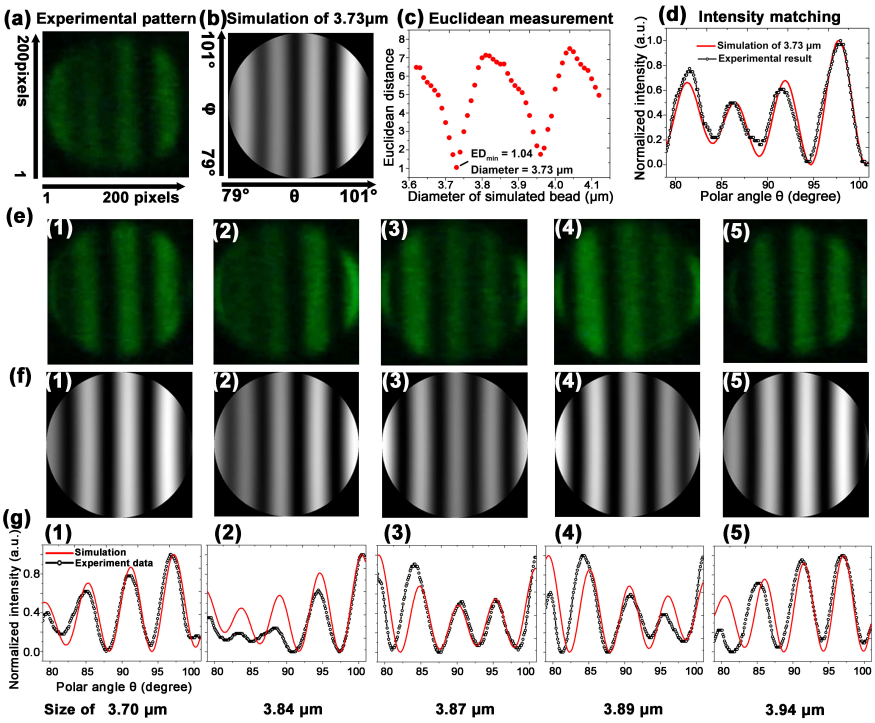

Fig. 4. A Euclidean distance based method for particle sizing with 2D light scattering patterns. Figure (a) is an experimental 2D light scattering pattern from a microsphere. (b) shows the Euclidean distance (ED) measurement for the experimental pattern (a). (c) is an simulation pattern for the bead with a diameter of 3.73 μm. (d) shows the spectra comparison between the experimental pattern (a) and simulation pattern (c). (e) shows the experimental patterns of microspheres, and (f) shows the simulation patterns drawn from a database. The results shown in (e) and (f) have the smallest Euclidean distances, and Fig. (g) shows their spectra comparisons, respectively.

The obtained 2D light scattering patterns were further analysed and compared with the stimulation results based on Mie theory. In our simulation, the refractive index of the microspheres is assumed to be 1.591 and the refractive index of surrounding medium is 1.334, at an excitation wavelength of 532 nm. For the experimental 2D light scattering pattern (as shown in Fig. 4(a)) from a homogeneous sphere, a horizontal scan along the 2D pattern at φ corresponding to 90° was performed. Then the Euclidean distance between the experimental and simulated data was calculated to evaluate the pattern similarity, as illustrated in Fig. 4(b). The microsphere size of the experimental pattern is determined to be the same as the simulation pattern (Fig. 4(c)) when the Euclidean distance is the smallest, where the simulation pattern is drawn from a database. The comparison of light scattering spectra at φ of 90° between experimental patterns (Fig. 4(a)) an simulation pattern (Fig. 4(c)) is plotted in Fig. 4(d), where the good matching of the two intensity curves validates our method. As shown in Fig. 4(e) and Fig. 4(f), the beads are approximated to be 3.70 μm, 3.84 μm, 3.87 μm, 3.89 μm, 3.94 μm in diameter with corresponding spectra matching results presented in Fig. 4(g) with the smallest Euclidean distances, respectively. Thus our Euclidean distance based method can be used for automatic particle sizing with submicron resolution.

Biomedical Optics EXPRESS

3.4. Automatic identification of senescent cells using a label-free light-sheet microfluidic cytometer

Our label-free light-sheet microfluidic cytometer was applied for label-free characterization of senescent and normal cells. The preparation of NHFs was performed as described previously [35]. They were maintained in Dulbecco Modified Eagle Medium (DMEM) supplemented with 10% fetal bovine serum and 100 units/mL penicillin-streptomycin in a humidified 5% CO_2 /95% air atmosphere at 37°C. The NHFs (at 17th passage) were treated with a single dose of 600 μM H_2O_2 to obtain SHFs. Both NHFs and SHFs were fixed with Immunology Staining Fix Solution (Beyotime, China) for 15 minutes at room temperature. The cells were then washed three times with phosphate buffer saline (PBS), and were resuspended in PBS before the light scattering experiments. In this work, the cell concentration was diluted to about 5 x 10^5/mL for obtaining 2D light scattering patterns from single cells. By using our light-sheet microfluidic cytometer, we obtained 240 2D light scattering patterns from single he control group (normal cells) and H_2O_2-treated group (senescent cells). Figure 5 shows the 2D patterns from the control group (normal cells) (Fig. 5(a)) and H_2O_2-treated group (senescent cells) (Fig. 5 (b)). It is noticed that the 2D patterns from NHFs and SHFs are characterized by speckles but differ in their structure, distribution and texture property.

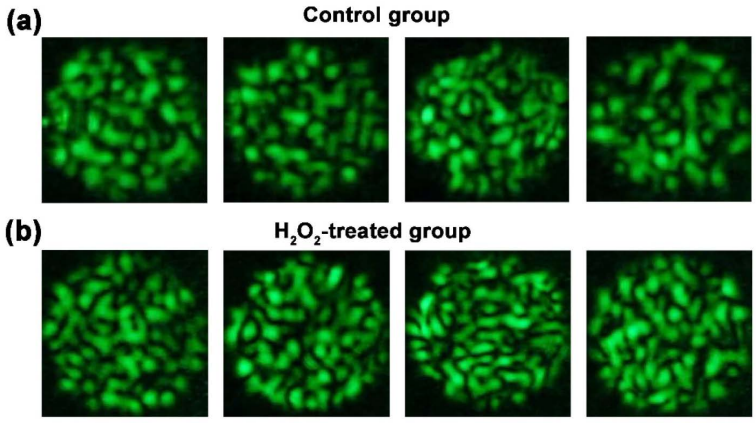

Fig. 5. Representative 2D light scattering patterns of single NHFs and SHFs obtained by the label-free light-sheet microfluidic cytometry. Figure (a) represent the 2D light scattering patterns of NHFs (control group) while the patterns in (b) are from single SHFs (H_2O_2-treated group).

For the automatic classification of NHFs and SHFs, a machine learning method (SVM) was adopted for the analysis of the 2D light scattering patterns [36]. Unlike the previously reported analysis for feature extraction from 2D patterns [37], a gray level co-occurrence matrices (GLCM) method that is based on the spatial distribution of pixels was employed in this report. The various GLCM parameters can be calculated as texture descriptors [38]. In this work, four parameters (contrast, correlation, energy and homogeneity) were computed for both the 2D patterns of NHFs and SHFs. These four features were used as eigenvectors for SVM classifier, which was based on a linear kernel function with 5-fold cross validation. The results for the label-free classification of normal and senescent cells are shown in Table 1. Here the sensitivity of 84.58% indicates the percentage for SHFs that are correctly identified, while the specificity that describes the recognition accuracy of NHFs is 91.67%. Therefore, we demonstrate that our light-sheet microfluidic cytometer with a microfabrication-free

Biomedical Optics EXPRESS

hydrodynamic focusing unit can perform label-free classification of NHFs and SHFs with a high classification accuracy rate of 88.13%.

Table 1. Label-free classification of NHFs and SHFs by SVM

Type	Total number	Correct number	Specificity	Sensitivity	Accuracy
NHFs	240	220	91.67%	–	88.13%
SHFs	240	203	—	84.58%	

Specificity means the recognition accuracy of negative category. Sensitivity describes the percentage of positive samples that are correctly classified. Accuracy is defined as the number of correctly identified NHFs and SHFs divided by the number of total NHFs and SHFs.

4. Discussion and conclusion

The hydrodynamic focusing unit we developed here is composed by two glass capillaries that are fixed by specially designed connectors. By changing the relative pressure of the pumping fluid and sheath fluid, our hydrodynamic focusing unit can provide a 3D focused fluid stream with a diameter changing from 19 μm to about 150 μm by using the inner capillary with inner diameters of 50 μm or 100 μm. It is importance to notice that the outer capillary is with a diameter of about 700 μm, and the sample fluid from the inner capillary is jetted into the outer capillary that is for sheath fluid. The flow rate of the 3D focusing stream can also be controlled by the relative pressure of the sample fluid and sheath fluid, and a flow rate changing from about 5 mm/s to 0.5 mm/s can be achieved. Compared with commercially available hydrodynamic focusing unit used in conventional cytometers, our hydrodynamic focusing unit costs much less. Secondly, our hydrodynamic focusing unit do not require microfabrication instruments and other clean room facilities, thus it is more accessible. Therefore, our microfabrication-free hydrodynamic focusing unit is disposable and may have versatile applications for different situations, such as for personalized medicine and mass production of microfluidic cytometer.

The light sheet illumination was adopted in this work, which is well suited for the integration with the hydrodynamic focusing for 2D elastic light scattering measurements. The thickness of the light sheet can be manipulated from about 15 μm to tens of micrometers, this could be aligned well with the 3D focused stream to excite only core of the hydrodynamically focused stream. In this case, background noise will be suppressed because only scatterers in the focused stream will be illuminated, thus the SNR for the 2D light scattering measurements can be improved. Furthermore, the large field of view and deep image depth of low NA objective require well confined sample fluid stream and illumination beam diameter for 2D light scattering measurements. The integration of light sheet with our 3D focusing unit solves this problem well.

Upon the development of a novel hydrodynamic focusing unit without microfabrication, which is coupled well with the light illumination, we provided in this work a next generation light-sheet microfluidic cytometry. Our light-sheet microfluidic cytometer was calibrated by measuring the 2D light scattering patterns from 3.87 μm (diameter) microspheres with an SD of 250 nm. It is expected that the 3.87 μm microspheres would contribute to different patterns because they have a discrete size distribution. However the size differentiation is challenging because of the optical diffraction limit, and the best resolution for the NA 0.25 objective is about 1.34 μm under visible light excitation. Here we developed an Euclidean distance based similarity method for particle sizing, where the simulated pattern is drawn from a data set. We demonstrated that the 3.87 μm microspheres with an SD of 250 nm can be well differentiated with a resolution that is much less than the best optical resolution of about 200 nm with visible light excitation. The particle sizing method based on Euclidean distance measurements that we developed here may find application in biomedicine, especially for the particle sizing in a liquid flow where conventional methods have certain limitations.

Biomedical Optics EXPRESS

Our light-sheet microfluidic cytometer has also been demonstrated for the identification of label-free senescent cells. Study of cell senescence is important for the understanding of senescence-related diseases. Conventional methods for cell senescence study rely on biomarkers. With the advancement of machine learning techniques, we developed an automatic, label-free method for the classification of SHFs from NHFs. The classification accuracy rate is as high as 88% which could be very practical for clinical applications. Considering that the H_2O_2 treated NHFs have a percentage of about 90% SHFs [29], our light-sheet microfluidic cytometer could provide a very high classification accuracy rate for automatic, label-free identification of senescent cells, and many other types of cells.

One promising future direction for the development of our label-free light-sheet microfluidic cytometer aims for high-throughput single cell analysis. With the current configuration, our cytometer has a throughput that is lower than the commercial flow cytometers [39]. This can be improved by using a high-speed imaging sensor, which however will lead to high cost. Another optional is to adopt the multichannel design to achieve parallel detection for high-throughput analysis [10, 40]. In this case, new machine learning algorithms may be developed for future applications in automatic, real-time analysis of high-throughput, label-free living cells.

In summary, we have developed a label-free light-sheet microfluidic cytometer with a microfabrication-free hydrodynamic focusing unit for the measurements of 2D light scattering from single cells. The light sheet illumination incorporates well with the 3D hydrodynamic focusing, especially for the improvements of the SNR for elastic light scattering measurements. By analysing the 2D light scattering patterns obtained with our light-sheet microfluidic cytometer, we have developed an Euclidean distance based method for particle sizing with submicron resolution. Our light-sheet microfluidic cytometer has the capability to obtain 2D light scattering patterns from flowing cells. By adopting SVM, a machine learning algorithm, for the analysis of the 2D light scattering patterns, an automatic classification of SHFs and NHF was realized with a classification accuracy rate of above 88%. This suggests that our label-free light-sheet microfluidic cytometer has potential for automatic, high-throughput analysis of senescence-related disease.

Funding

National Natural Science Foundation of China (NSFC) (81271615); Qilu Youth Scholar Startup Funding of Shandong University; Multidisciplinary Precision Oncology Project of Shandong University.

Disclosures

The authors declare that there are no conflicts of interest related to this article.